Mon. Not. R. Astron. Soc. **398,** 591–606 (2009) doi:10.1111/j.1365-2966.2009.15133.x

The origin of the light distribution in spiral galaxies

P. Sánchez-Blázquez,[1,2★] S. Courty,[1] B. K. Gibson,[1] and C. B. Brook[1]

[1] *Jeremiah Horrocks Institute for Astrophysics and Supercomputing, University of Central Lancashire, Preston PR1 2HE*
[2] *Instituto de Astrofísica de Canarias, c/Vía Láctea s/n, E38205, La Laguna, Tenerife, Spain*

Accepted 2009 May 24. Received 2009 April 25; in original form 2009 March 1

ABSTRACT

We analyse a high-resolution, fully cosmological, hydrodynamical disc galaxy simulation, to study the source of the double-exponential light profiles seen in many stellar discs, and the effects of stellar radial migration upon the spatiotemporal evolution of both the disc age and metallicity distributions. We find a 'break' in the pure exponential stellar surface brightness profile, and trace its origin to a sharp decrease in the star formation per unit surface area, itself produced by a decrease in the gas volume density due to a warping of the gas disc. Star formation in the disc continues well beyond the break. We find that the break is more pronounced in bluer wavebands. By contrast, we find little or no break in the mass density profile. This is, in part, due to the net radial migration of stars towards the external parts of the disc. Beyond the break radius, we find that ∼60 per cent of the resident stars migrated from the inner disc, while ∼25 per cent formed *in situ*. Our simulated galaxy also has a minimum in the age profile at the break radius but, in disagreement with some previous studies, migration is not the main mechanism producing this shape. In our simulation, the disc metallicity gradient flattens with time, consistent with an 'inside-out' formation scenario. We do not find any difference in the intensity or the position of the break with inclination, suggesting that perhaps the differences found in empirical studies are driven by dust extinction.

Key words: methods: numerical – galaxies: abundances – galaxies: kinematics and dynamics – galaxies: spiral – galaxies: stellar content – galaxies: structure.

1 INTRODUCTION

Since 1940, it has been known that the stellar disc light in spiral galaxies decreases exponentially with radius (Patterson 1940; Freeman 1970). This is thought to be the result of the initial angular momentum distribution of the gas cloud that collapsed to form the disc (Fall & Efstathiou 1980; Dalcanton, Spergel & Summers 1997; Mo, Mao & White 1998; Ferguson & Clarke 2001; van den Bosch 2001). However, since the pioneering work of van der Kruit (1979), it has become clear that this exponential profile does not extend to arbitrarily large radii in the majority of disc galaxies. Pohlen & Trujillo (2006) and Erwin, Pohlen & Beckman (2008) showed – for later and earlier types, respectively – that, in fact, the galaxies for which this happens represent a minority, identifying three classes of surface brightness behaviour in the outskirts of disc galaxies: ∼60 per cent of the galaxies show a deficit of light with respect to an extrapolated singular exponential (Type II); ∼30 per cent show an excess of light in the outskirts with respect to a singular exponential (Erwin, Beckman & Pohlen 2005; Pohlen & Trujillo 2006, Type III); while only ∼10 per cent show pure exponential profiles (Bland-Hawthorn et al. 2005; Pohlen & Trujillo 2006; Erwin et al. 2008, Type I) out to $\gtrsim$10 scalelengths.[1] Further departure from the notion of the 'disc-as-exponential' paradigm leads to even more elaborate classifications based upon, for example, the position of the 'break' with respect to the Outer Lindblad Resonance (OLR) of the bar (for Type II) or the exact shape of the surface brightness profile in the outskirts (for Type III) (e.g. Pohlen & Trujillo 2006; Erwin et al. 2008).

The break radius ($R_{\rm br}$) or the radius at which the light profile starts to deviate from a pure exponential is empirically seen to occur at ∼1.5–4.5 disc scalelengths (Pohlen & Trujillo 2006). Outside the break, the surface brightness does not immediately drop to zero, but follows a second (different) exponential (de Grijs, Kregel & Wesson 2001; Pohlen 2002). The fact that such breaks are very common, at least in late-type galaxies (Beckman, lrwin & Pohlen 2006), indicates that they either form easily or survive for significant periods of time. The exact causes though, 30 years on from the identification of this 'break' phenomenon, remain unclear. The leading candidates can be divided broadly into those related to angular momentum conservation and those related to a star formation threshold.

★E-mail: psanchez-blazquez@uclan.ac.uk

[1] These percentages are very dependent upon the morphological class of the galaxy (see Beckman et al. 2006).

In the case of the former, it can be shown that *if* angular momentum redistribution does not occur in the disc, the outermost stellar radius will reflect the maximum value of the angular momentum of the baryonic material (that of the protogalaxy) (van der Kruit 1987). However, numerical simulations have shown that non-axisymmetric instabilities *do* drive a substantial redistribution of angular momentum in the disc (Debattista et al. 2006) and that, in fact, this can be a responsible agent for a break. This is because the angular momentum redistribution leads to an increase in both the central densities and disc scalelengths. As the angular momentum redistribution cannot act efficiently to arbitrarily large radius, a break in the surface mass density distribution results.

Alternatively, breaks may be due to the effect of star formation thresholds (Kennicutt 1989). Within this latter scenario, the break radius would be located where the density of the gas is lower than the critical value for star formation. The existence of extended ultraviolet (UV) discs (Gil de Paz et al. 2007; Thilker, Bianchi & Meurer 2007), the lack of correlation between Hα 'cut-offs' and optical disc breaks (Pohlen et al. 2004; Elmegreen & Hunter 2006) and the exponential decay of the light outside the break, however, have all been used as arguments against this picture. That said, Elmegreen & Hunter (2006) showed that a double-exponential profile *may* result from a multicomponent star formation prescription, where turbulent compression in the outer parts of the disc can allow for cloud formation and star formation despite subcritical densities. More recently, models have shown that redistribution of stellar material in the disc can also lead to exponential profiles outside the star-forming disc's break radius (Roškar et al. 2008b).

Not surprisingly, hybrid models have been suggested which combine aspects of both the pictures. For example, van den Bosch (2001) investigated a combination of the collapse and the threshold model, claiming that gas breaks are a direct consequence of the angular momentum of the protogalaxy while the stellar breaks are determined by a star formation threshold.

While each proposed model appears capable of explaining the presence of disc breaks, it is equally important that any successful hypothesis also takes into account the fact that (i) breaks are not seen in *all* galaxies (Barton & Thompson 1997; Weiner et al. 2001; Bland-Hawthorn et al. 2005); (ii) breaks are seen in discs of *all* morphological types, from S0 (Erwin et al. 2008) to Sm (e.g. Kregel, van der Kruit & de Grijs 2002; Pohlen & Trujillo 2006) and even in irregular galaxies (Hunter & Elmegreen 2006) – albeit, not with the same frequency and (iii) breaks are observed out to redshift $z \sim 1$ (Pérez 2004; Trujillo & Pohlen 2005; Azzollini, Trujillo & Beckman 2008b). Recent observational studies have now imposed additional constraints on the models for break formation. For example, de Jong et al. (2007) have shown that the break position is independent of stellar age, a result compatible with that of Bakos, Trujillo & Pohlen (2008), who found the position of the break to be independent of the photometric band. It has also been found that the prominence or intensity of the break decreases with increasing distance from the galactic mid-plane (de Jong et al. 2007) and for older stellar populations (Azzollini, Trujillo & Beckman 2008a; Bakos et al. 2008).

Furthermore, the recent work of Roškar et al. (2008b) has demonstrated the importance of stellar migrations in defining the final mass density and surface brightness density profiles of disc galaxies. The reorganization of stars in the disc can have important consequences for the observational constrains used for the chemical evolution models, as the age–metallicity relation or the metallicity distribution, as previously shown by several studies (e.g. Haywood 2006, 2008; Roškar et al. 2008a; Schönrich & Binney 2009).

Previous work in this area has concentrated upon somewhat idealized scenarios of isolated galaxies. The advantage of this approach is that higher resolution can be achieved more readily, with a greater associated exploration of parameter space. However, such an approach necessarily carries with it the disadvantage of not being able to take into account various processes such as the cosmological infall of gas and/or the interactions with other galaxies that are intrinsic to the hierarchical assembly paradigm. Indeed, interactions with satellites can have an important influence in shaping the disc, as suggested by simulations (e.g. Peñarrubia, McConnachie & Babul 2006; Younger et al. 2007) and should not be ignored. Our work aims to fill this hole by addressing the possible physical origins of the two-component surface brightness profiles, but now within a cosmological context. We will examine the likelihood that such profiles are the consequence of dynamical processes, star formation processes or a combination of the two.

2 SIMULATION DETAILS

Our model disc was realized using multiresolved, cosmological simulations generated with the *N*-body, hydrodynamical code RAMSES (Teyssier 2002) which is based upon an adaptive mesh refinement (AMR) technique. RAMSES includes gravitation, hydrodynamics, radiative cooling and heating processes, immersed within a uniform, Haardt & Madau (1996) ionizing radiation field. In addition to solving the Euler equations with a net cooling term, the RAMSES includes a phenomenological treatment of star formation, which contributes directly to the chemical enrichment of the interstellar and intergalactic medium via subsequent Type II supernovae.[2] The spatiotemporal evolution of the gas metal abundance, as well as the redshift-dependent photoionizing background, is consistently accounted for in the computation of the net cooling rates of the gas (Courty & Teyssier, in preparation). This combined contribution has been fit using the CLOUDY photoionization code (Ferland et al. 1998).

The star formation prescription within RAMSES is described in detail by Dubois & Teyssier (2008); only a brief summary is provided in what follows. Star formation is permitted in cells whose density is higher than a given threshold, according to the following rate: $\dot{\rho}_* = -\rho/t_*$, where the star formation time-scale is proportional to the local free-fall time, $t_* = t_0(\rho/\rho_0)^{1/2}$. As in Dubois & Teyssier's work, we set this time-scale to $t_0 = 8$ Gyr, with an associated density threshold for star formation of $\rho_0 = 0.1$ H cm^{-3}. Kinetic feedback of supernovae energy to the surrounding interstellar medium (ISM) is modelled with a blast-wave solution that essentially mimics the expansion of superbubbles whose radius is fixed to two cells. Thermal feedback is accounted for by using a polytropic equation of state in the high-density regions. The amount of gas then turned into stellar material in each eligible gas cell is $m_*(1 + \eta_{SN} + \eta_W)$, where the mass locked in long-lived stars is m_*, and $m_*(\eta_{SN} + \eta_W)$ is the mass carried away by the blast wave, with the wind-driving parameter $\eta_W = 1$, and the mass fraction of stars recycled into supernovae ejecta $\eta_{SN} = 0.1$. Photometric properties of the resulting stellar populations were derived by assuming that each star particle was a single stellar population, and then applying the models

[2] The current implementation of chemistry within RAMSES is restricted to the global metal content (Z), under the assumption of the instantaneous recycling approximation; an extension to RAMSES which relaxes this approximation and includes the effects of Type Ia supernovae and asymptotic giant branch stars is currently under development (Few et al., in preparation).

of Bruzual & Charlot (2003) with a Salpeter (1955) initial mass function and the Bertelli et al. (1994) isochrones.

Our simulation starts at $z = 999$ and continues to $z = 0$ in a Λ cold dark matter (ΛCDM) universe with the following cosmological parameters, $\Omega_\Lambda = 0.7$, $\Omega_{\rm m} = 0.3$, $\Omega_{\rm b} = 0.045$, $\sigma_8 = 0.9$ and $H_0 = 73\,{\rm km s^{-1}\,s^{-1}\,Mpc^{-1}}$. To carry out cosmological simulations of disc galaxies at the sub-kpc scale, a multiresolved approach was adopted. Candidate dark matter haloes were chosen in a low-resolution, large-scale structure simulation. The size of this ΛCDM simulation was $20\,h^{-1}$ Mpc, contains 128^3 dark matter particles and was generated with RAMSES as part of the Horizon Project.[3] Our multiresolved simulation used three nested boxes whose initial conditions were centred on our candidate halo and whose resolution ranged from 128^3 in the external part of the computational volume to 512^3 for the most nested box. The latter resolution is also one of the coarse grids in the central area, and the adaptive mesh nature of RAMSES was employed to refine a further seven levels, thereby reaching a spatial resolution of 435 pc by $z = 0$. Dark matter particles have a mass of $6 \times 10^6\,{\rm M_\odot}$ and the initial gas mass per cell was $\sim 10^6\,{\rm M_\odot}$.

As noted in Gibson et al. (2009), the selection of the candidate halo was made without any pre-conceptions regarding spin λ or triaxiality T. Care was taken though to ensure that the final halo was not contaminated by low-resolution dark matter particles up to at least five virial radii. The disc galaxy discussed here sits within a low-spin ($\lambda = 0.02$), mildly oblate triaxial ($T = 0.32$) halo of dynamical mass $7.6 \times 10^{11}\,{\rm M_\odot}$. For redshifts $z < 2.3$, the rotational axis of the disc could be aligned readily using the angular momentum vector of the gas cells; the analysis which follows is therefore restricted to $z < 2.3$. Further technical details of the simulation and alignment process are forthcoming (Courty et al., in preparation).

3 CHARACTERISTICS OF THE DISC

Hydrodynamical simulations of galaxies within the canonical hierarchical structure assembly framework are known to have a number of difficulties in reproducing disc-dominated galaxies (e.g. Abadi et al. 2003a; Springel & Hernquist 2003; Bailin et al. 2005; Okamoto et al. 2005; Governato et al. 2007; Scannapieco et al. 2008). A major problem is that baryons condense early and then transfer a significant fraction of their angular momentum to the dark matter as the final galaxy assembles (Navarro & White 1994). As a result, these galaxies contain a significant fraction of their final baryonic mass in a spheroidal-like component supported primarily by velocity anisotropy, with consequent bulge-to-disc ratios in excess of those encountered in late-type spirals today.

To derive the bulge-to-disc ratio of our simulated galaxy, we categorize the stars as 'disc' or 'spheroid' following Abadi et al. (2003b) and Scannapieco et al. (2009). We derive the distribution of the circularity parameter ϵ [where $\epsilon = j_z/j_{\rm cir}$ and j_z is the z-component of the specific angular momentum of each star, where the z-axis is the symmetry axis and $j_{\rm cir}$ is the angular momentum expected for a circular orbit at the same radius, r – i.e. $j_{\rm cir} = r v_{\rm cir}(r)$]. Fig. 1 shows the ϵ distribution of all stellar particles within a sphere of radius of 20 kpc at $z = 0$ (black). We have marked, with different colours, those particles inside a sphere of radius 1.5 kpc (red), and those with radius $3 < r < 15$ kpc and within 3 kpc of the disc mid-plane (green). Considering a stellar disc composed of stars with $r < 15$ kpc, $|z| < 3$ kpc and $0.8 < \epsilon < 1.2$, and including only those

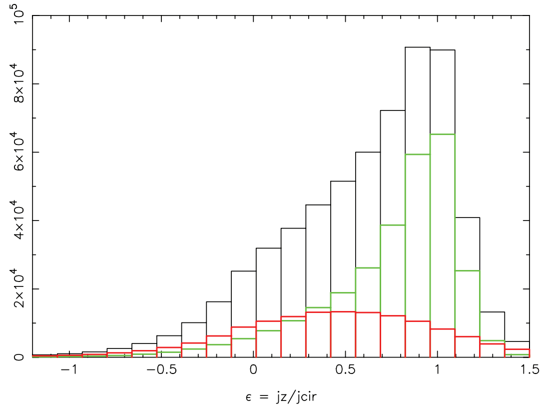

Figure 1. Distribution of $\epsilon = j_z/j_{\rm cir}$ for all stars within a sphere of $r < 20$ kpc (black line), within a sphere of 1.5 kpc (red line), and all those with $3 < r < 15$ kpc and distance from the mid-plane $< |3|$ kpc (green line).

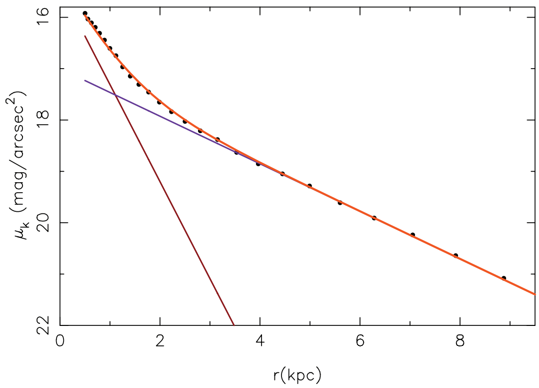

Figure 2. K-band surface brightness profile of our simulated disc, plotted out to ~3 disc scalelengths. The fitted profiles of the disc (exponential law, shown in purple) and the bulge (Sersic law, shown in dark red) are overlaid, along with the sum of the two (shown in orange).

stars rotating in the plane of the disc (with $\cos\alpha > 0.7$, where α is the angle between the angular momentum vector of the particle and the z-axis, after Scannapieco et al. 2009), the disc-to-total ratio in our galaxy – measured as the ratio between the stellar mass on the disc and the total stellar mass – is 0.37. Put another way, the bulge-to-disc ratio is, not surprisingly (and in keeping with the aforementioned particle-based disc simulations), large with respect to that observed in late-type spirals (Sb-Sd), being more consistent with the ratio expected for an early-type (Sa-S0) galaxy. Fig. 2 shows a bulge-to-disc decomposition of our simulation, using the K-band light profile and employing an exponential law for the disc and a Sersic law for the bulge. The fit was done in an iterative manner, following MacArthur, Courteau & Holtzman (2003), resulting in a photometric bulge-to-disc ratio of $\log(B/D) = -0.5$, consistent with that expected for an early-type (Sa-S0) galaxy (e.g. morphological type $T \sim 3$; Simien & de Vaucouleurs 1986).

The stellar bulge associated with our simulated disc is partially supported by rotation (with $V_{\rm rot}/\sigma \approx 0.5$, where $V_{\rm rot}$ is the maximum rotational velocity). In the simulation here, much as for the Milky Way bulge (admittedly, perhaps just coincidentally), $V_{\rm rot} = 70\,{\rm km\,s^{-1}}$.

Fig. 3 shows a density map of the stellar disc from two different perspectives (face-on and edge-on). The disc extends to ~20 kpc, with an exponential scalelength (measured in the V band) of ~3.2 kpc, consistent with values found for late-type spirals such

[3] http://www.projet-horizon.fr

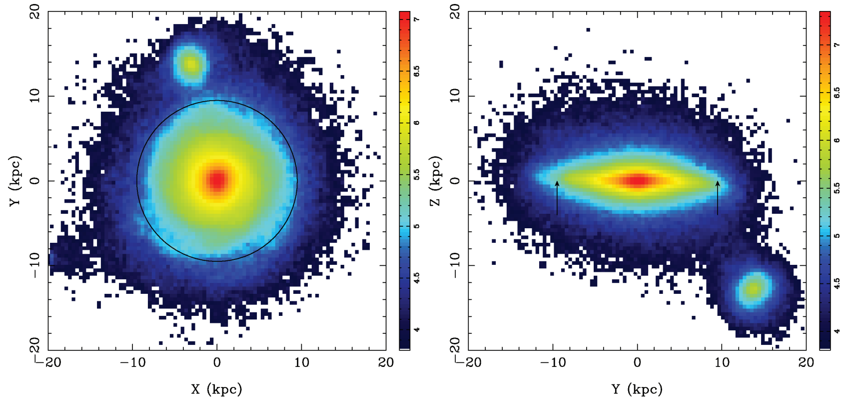

Figure 3. Stellar density projections of the disc (left-hand panel: face-on; right-hand panel: edge-on). A 40 × 40 kpc region is shown in both the panels. The circle in the left-hand panel and the arrows in the right-hand panel indicate the position of the break radius (see Section 4).

as the Milky Way (e.g. Jurić et al. 2008 suggest a scalelength for the Milky Way's disc of ∼2.6 kpc).

While the stellar disc extends to ∼20 kpc, the bulk of our analysis is restricted to stars within a radius of 15 kpc. This is mainly due to the 'law-of-diminishing-returns' in the outskirts where the number density of stellar particles decreases dramatically and the rms dispersion of relevant azimuthally averaged quantities begins to increase rapidly. Furthermore, considering only particles inside this 15 kpc radius means we also reduce the possible contamination from cospatial stellar halo particles.

We end by noting that all 'error bars' plotted throughout the paper are derived from the rms associated with the mean values from eight arbitrary octants of the disc.

4 CHARACTERISTICS OF THE DISC BREAK

The first two rows of Fig. 4 show the evolution of the azimuthally averaged surface brightness profile in the V band and the total stellar surface density profile, respectively, at five different epochs from $z = 2$ to 0. It can be seen that the disc has already developed a break by $z \sim 1$ in the surface brightness profile and maintained its presence through to $z = 0$. We fit simple functional forms [$\mu(R) = \mu_0 + 1.086 \times R/h$] to the inner and outer exponentials and consider that the break occurs at the position where the functions intersect. At redshift $z = 0$, the break radius is $R_{\rm br} \approx 9.5$ kpc (i.e. ∼2.9 disc scalelengths). The break intensity – measured as the angle between the inner and outer exponential profiles – changes with redshift,

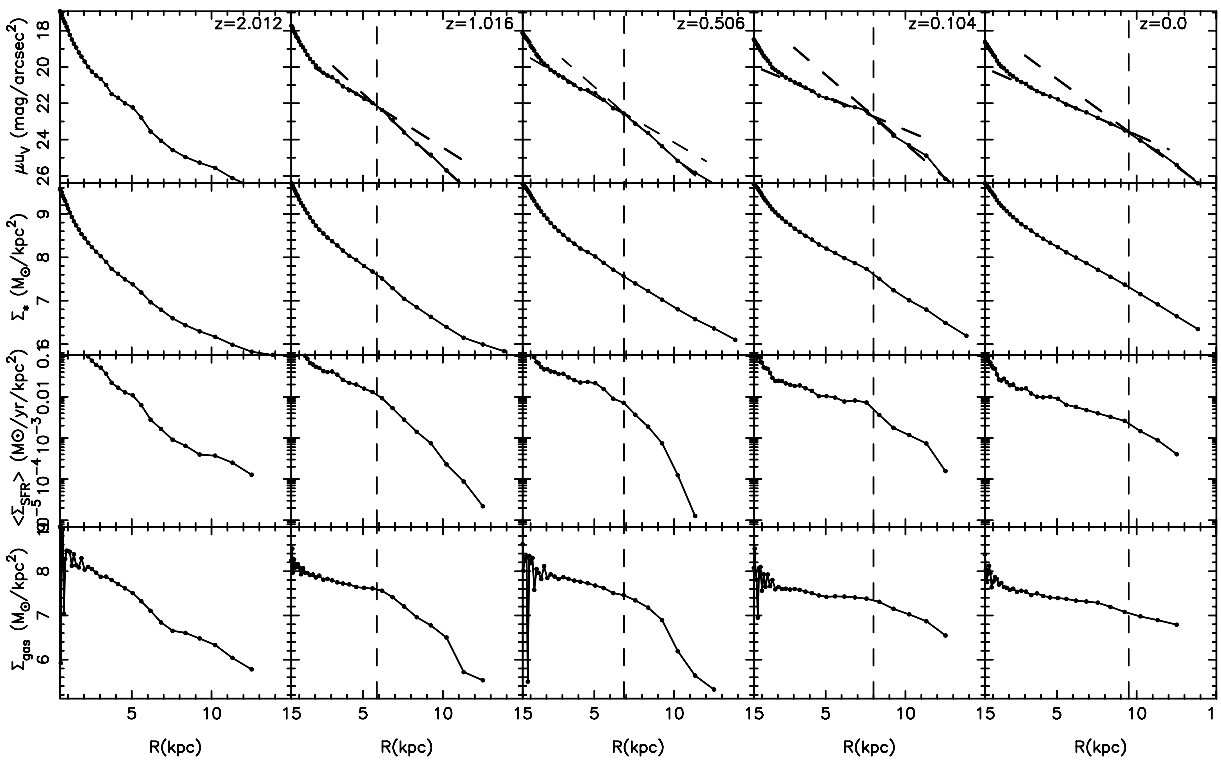

Figure 4. Evolution with redshift – as indicated in the inset to each panel – of the V-band surface brightness profile (first row), total stellar surface density profile (second row), SFR surface density profile (third row) and gas surface density profile (fourth row), all on logarithmic scales. The profiles were derived using all stars with $r < 15$ kpc and $|z| < 3$ kpc. Dashed lines represent fits to the inner and outer exponentials in the V-band surface brightness profile. The break radii correspond to the intersection point of these two exponentials, and are noted by the vertical dashed lines in each panel.

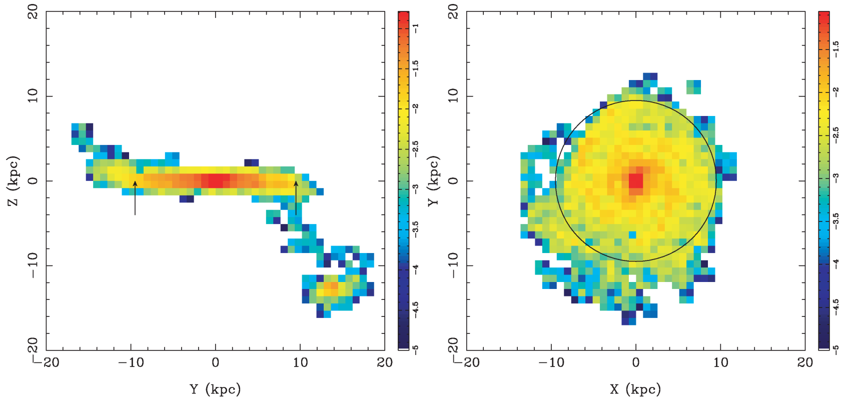

Figure 5. Edge-on and face-on two-dimensional projections of the present-day integrated (over the last 100 Myr) SFR for our cosmological disc. For the face-on projection, only the stars at a distance of 5 kpc from the plane are included, to avoid contamination from the companion. The total line of sight in the edge-on projection is 40 kpc.The vertical arrows (edge-on) and circle (face-on) correspond to the position of the break radius in the V-band surface brightness distribution.

but not in any obvious monotonic/systematic manner. It can also be seen that the break is much shallower in the total stellar mass surface density distribution. In fact, in most snapshots it is almost non-existent, a point to which we return in Section 7.1.

Fig. 5 shows spatially resolved two-dimensional star formation rate (SFR) maps of our simulation at z=0. The break radius is denoted by the vertical arrows (edge-on view) and circle (face-on view); an immediate point of interest is that there remains measurable star formation outside the break radius. This star formation is not axisymmetric, with star formation extending beyond $R_{\rm br}$ on one side, in particular. Such star formation in the outer disc (beyond the break radius) has been observed in many galaxies (Ferguson 1998; Ferguson et al. 1998; Thilker, Bianchi & Boissier 2005; Gil de Paz et al. 2007; Thilker et al. 2007). Before assessing the physical origins driving the formation of the break in the surface brightness profile, we first review the main observational characteristics, to determine if our light profile is a fair representation of those observed in real galaxies.

4.1 Dependence of the break upon distance from the mid-plane

In the case of NGC 4244, de Jong et al. (2007) show that the break occurs at the same radius independent of height above the mid-plane. They further demonstrate that the intensity of the break decreases with height above the plane. Fig. 6 shows the surface brightness profiles derived from our simulation, in the Sloan Digital Sky Survey (SDSS) g band, for samples of stellar particles at different distances from the plane. The empirical characteristics seen by de Jong et al. (2007) are similarly seen in the simulation – specifically, the break radius position does not change with distance from the mid-plane, but it gets shallower.

4.2 Dependence of the profile upon photometric band

Different photometric bands are sensitive to different stellar populations. While the main contributors to the luminosity in the blue bands are the young stars,[4] this contribution decreases for the redder

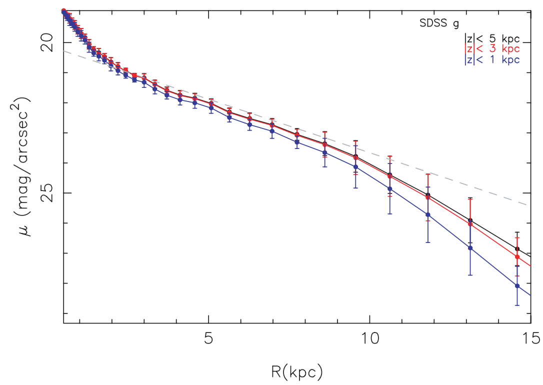

Figure 6. Azimuthally averaged surface brightness profiles in the SDSS g band, integrating particles within 1, 3 and 5 kpc from the mid-plane, as indicated in the inset. Error bars represent the rms dispersion between the mean values found in eight arbitrary octants of the disc.

bands. Interestingly, Bakos et al. (2008) have found recently that the position of the break is independent of the photometric bandpass employed to obtain the surface brightness profile, although break is shallower in the redder bandpasses. These results suggest that the break is due mainly to a truncation in the profile of the young stars and that the profile of the old stars should not show the same departure from a pure exponential.

Fig. 7 shows the surface brightness profiles of the stellar disc in the same two photometric bands (g and r) used in the empirical study of Bakos et al. (2008), in addition to the redder K band. In our simulation, the break appears at the same position (∼9.5 kpc) but, in agreement with the observations, is also shallower in the redder band (Ks) than it is in the bluer one (g). Furthermore, Bakos et al. (2008) transform the surface brightness profiles into total stellar mass density profiles, using mass-to-light ratios inferred from the colours, following the prescriptions of Bell et al. (2003). This process is admittedly not free of uncertainties, but, at face value, their results suggest that the mass density profile does not show a break, in agreement with that found for our simulated disc (see Fig. 4).

Fig. 8 shows the stellar mass surface density distribution in our simulated disc for stars of different ages. While the position of the break is the same for those stellar populations showing a break in the stellar density distribution, not all stars show this truncated

[4] Other hot stellar populations, including blue horizontal branch stars and blue stragglers, may provide an additional contribution in some systems (see e.g. Rose 1985; Maraston & Thomas 2000; Trager et al. 2005).

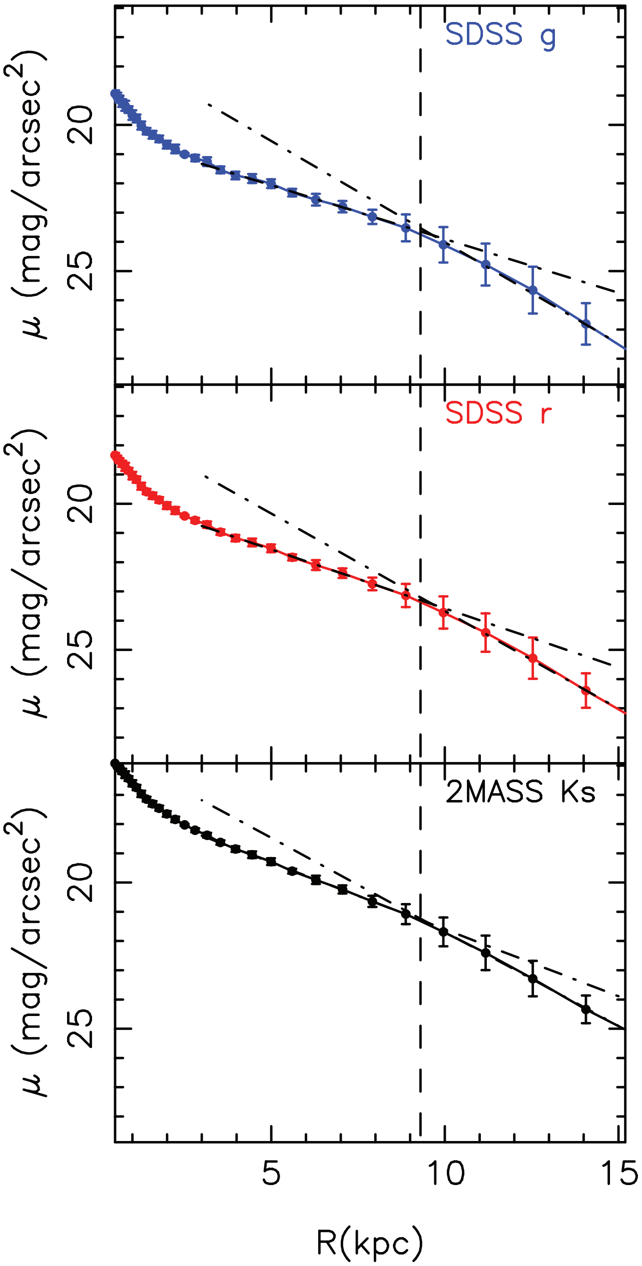

Figure 7. Surface brightness profiles measured in three different bands, as indicated in the inset to each panel. Dashed vertical lines show the position of the break radius, while the dash–dotted lines represent the fits to the inner and outer exponentials.

density profile. In particular, stars older than ∼8 Gyr show, if anything, a slightly 'upbending' profile. This latter result agrees with a number of observational studies: Davidge (2003) studied the stellar populations in the outskirts of NGC 2403 and M33, showing that while the number of young main-sequence stars presents a 'downbend' with radius, the number density of the more evolved stars in the red and asymptotic giant branch phases does not. Similar results were also obtained by Galleti, Bellazzini & Ferraro (2004) for M33. Conversely, for the case of NGC 4244, de Jong et al. (2007) claim a sharp break even when only red giant stars (old stars for a constant star formation history) are considered. This issue clearly needs resolving with a larger sample of galaxies.

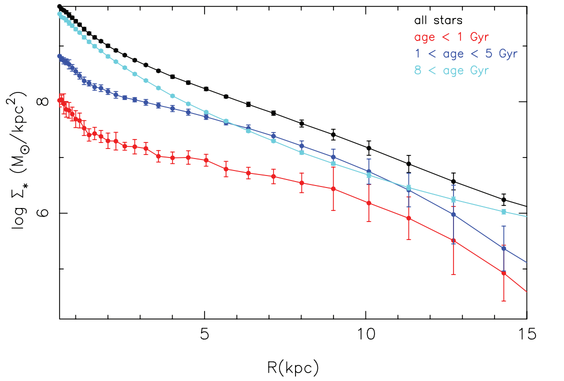

Figure 8. Stellar surface density profiles for stars of different ages, as noted in the inset. The intensity of the break decreases with increasing age of the stellar population under consideration, with old stars showing an 'upbend' at large radii. The total stellar surface density profile is consistent with a pure exponential out to ∼5 exponential scalelengths.

4.3 Colour profiles

Recently, Bakos et al. (2008), for the local universe, and Azzollini et al. (2008b), out to redshift $z \sim 1.1$ (see also Jansen et al. 2000), have found that the colour gradients of galaxies with Type II truncations are different from those with Type I or pure exponential profiles (recalling the nomenclature introduced in Section 1). In particular, galaxies showing Type II truncations have a 'U-shaped' colour profile, with the minimum (bluest colour) at the position of the break.

Fig. 9 shows our predicted colour profile at four different epochs from $z = 1$ to 0. In agreement with the observations, our simulated disc also shows a U-shaped profile with the bluest colours near the position of the break.

4.4 Age and metallicity profiles

Colours are difficult to interpret in terms of simple stellar populations due to the well-known 'age–metallicity degeneracy' (Worthey 1994); in principle, the colour profile could be an effect of age, metallicity or a combination of both. Fig. 10 shows the mass-weighted stellar age and metallicity gradients for the final output of our simulation. It can be seen that the age profile presents a minimum at roughly the position of the break. However, the metallicity profile is remarkably smooth all the way out ∼15 kpc, without any visible change at the break radius. Therefore, the U-shape of the colour profiles seen in previous section is due to an age effect, and not due to a metallicity effect.

4.5 Evolution of the break with redshift

Several studies have now analysed the empirical evolution of the break radius with redshift (Pérez 2004; Trujillo & Pohlen 2005; Azzollini et al. 2008b). Using a sample in excess of 200 galaxies, for example, Azzollini et al. suggest that, for a given stellar mass, the radial position of the break has increased with cosmic time by a factor of 1.3 ± 0.1 between $z \sim 1$ and 0. They also found that, in the same period of time, the evolution of the surface brightness level in the rest-frame B band at the break radius ($\mu_{\rm br}$) has decreased by 3.3 ± 0.2 mag arcsec^{-2}.

Because the mass of our simulated galaxy evolves with redshift, we cannot directly compare the evolution of these parameters for a galaxy with a given mass. For this reason, we re-analysed these data

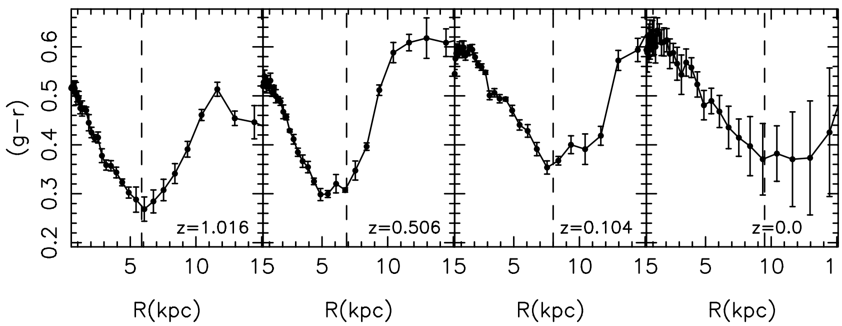

Figure 9. Colour profiles for several outputs of our simulation from $z = 1$ to 0. Dashed lines in each panel indicate the position of $R_{\rm br}$ in the V-band surface brightness profile (recall Fig. 4). Error bars reflect the rms dispersion of the mean azimuthally averaged colour in randomly selected octants of the disc. The colour profiles show a minimum at the break radius, in agreement with observation.

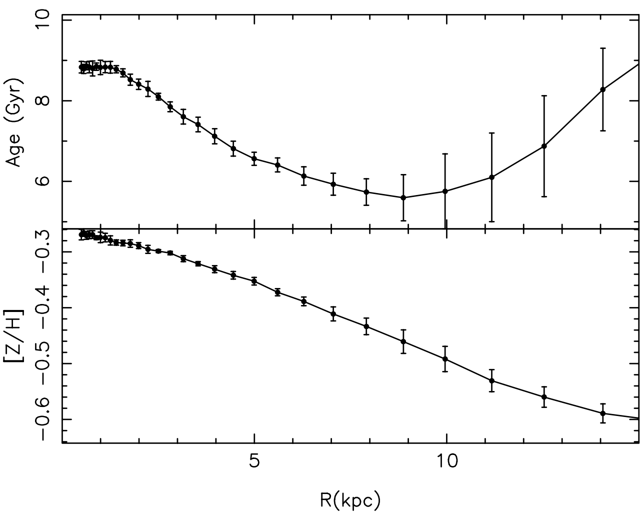

Figure 10. Mass-weighted age and metallicity gradients for our simulated disc at $z = 0$.

(kindly provided by the authors). We separated the observational data into three redshift bins and fitted, at each redshift, a linear relation between $R_{\rm br}$, $\mu_{\rm br}$ and the mass of the galaxies, in an identical fashion to that done by Azzollini et al. (2008b). Using the linear fit, we measured the predicted values of $R_{\rm br}$ and $\mu_{\rm br}$ for a galaxy with the same mass as our disc at each of the different redshift bins (note that the mass is different at each redshift) and their associated rms dispersions. Fig. 11 shows the predicted evolution of $R_{\rm br}$ and $\mu_{\rm br}$ in the B band for our simulated disc, compared to the observed data. It can be seen that the evolution of these parameters within our simulated disc is very similar to that which is observed.

4.6 Age and metallicity distributions in the outskirts

Studies of stellar population in the outskirts of discs have found stellar populations which are of old-to-intermediate ages, with metallicity distributions peaking at relatively high metallicities ([Fe/H] ~ -0.7) [e.g. Ferguson & Johnson 2001 (M31); Davidge 2003 (NGC 2403, M33); Galleti et al. 2004 (M33)]. It has been suggested that these properties are not expected in CDM models (e.g. Ferguson & Johnson 2001), where the disc grows inside-out and at relatively recent epochs ($z \lesssim 1$). Fig. 12 shows the age and metallicity distributions of stars with $R_{\rm br} < r < 15$ kpc in our simulated disc. There is a very large scatter in the ages of the stars, and a significant fraction of the stellar population has ages in excess of $\sim$8 Gyr. The peak of the metallicity distribution is near [Fe/H] ~ -0.5 – i.e. even larger metallicities than that normally observed in the outskirts of galaxies. However, it should be noted that the 'observed' metallicities are inferred via the use of colour–magnitude diagrams. When dealing with photometric metallicities, one must bear in mind that the underlying age distribution may affect the derived metallicity distribution. All of the studies cited above obtained their metallicities by comparing with the sequences of old Milky Way globular clusters. If a scatter in age is allowed, with a larger fraction of young stars (as we obtain in our simulation), the metallicity distribution will be skewed towards higher values and more closely resemble our derived distribution. We note that our metallicity distribution has a metal-poor tail, as reported in some empirical studies (e.g. Galleti et al. 2004).

5 BREAK FORMATION

As foreshadowed in Section 1, there is no clear consensus regarding the underlying physical mechanism responsible for the surface

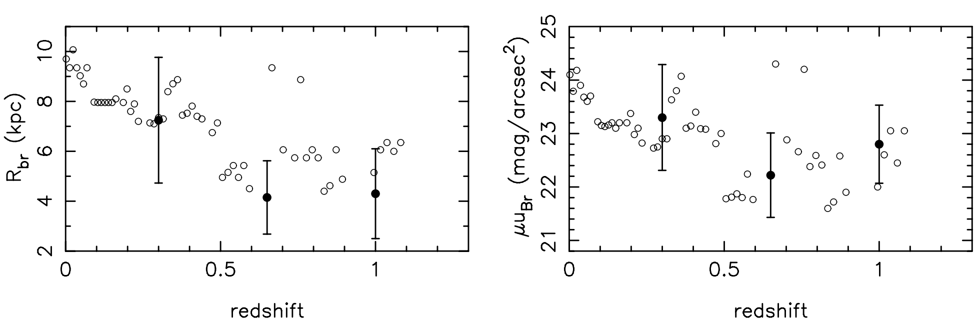

Figure 11. Predicted evolution with redshift of $R_{\rm br}$ and $\mu_{\rm br}$ (open circles) compared to the observed values from Azzollini et al. (2008) (filled circles with error bars). The error bars show the rms dispersion of the measured values for galaxies in a given redshift bin and mass bin.

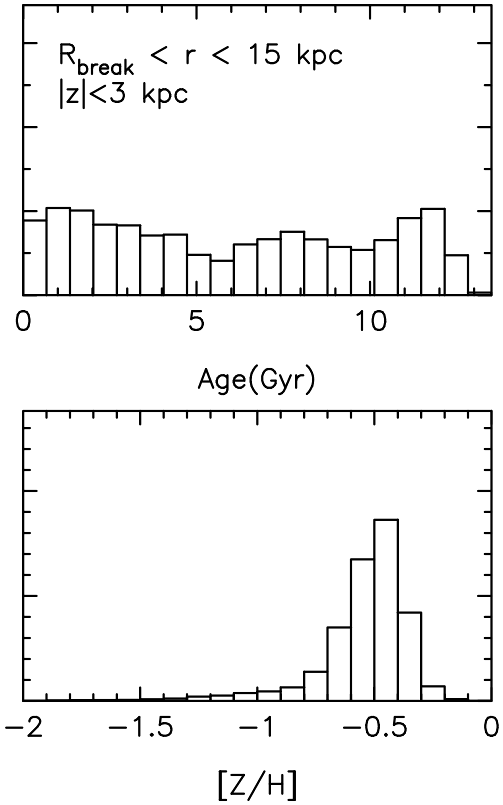

Figure 12. Age and metallicity distributions for the stars with radius $R_{\rm br} < r < 15$ kpc and $|z| < 3$ kpc.

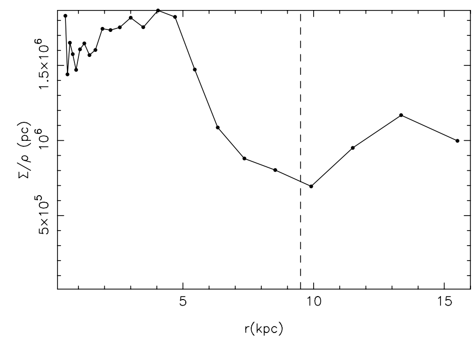

Figure 13. Ratio between the surface mass density and the volume density, as a function of Galactocentric radius at redshift $z = 0$, in our simulated disc galaxy. The position of the break in the surface brightness profile is indicated with a dashed line.

brightness profile breaks observed both locally and at high redshift. Broadly, there are two categories of theories – those related with the angular momentum distribution of the stars and those related to star formation thresholds.

In our simulated disc, the break is seen in the light profile, but not in the stellar mass density profile. This indicates (or at least suggests) that the break in our disc is likely related to a change in the stellar population properties and, therefore, with a star formation threshold. The third and fourth rows of Fig. 4 show the SFR density (with the SFR averaged over the last 1 Gyr) and gas surface density profiles, respectively. Examining Fig. 4, we can see that the gas surface density at the break radius is not the same at all redshifts. For example, at $z = 2.01$ there is no clear break in the surface brightness profile, despite the gas surface density reaching values significantly below the star formation threshold. This would seem to contradict the aforementioned star formation threshold scenario as the driver behind the break. In Roškar et al. (2008b), the reason for the break was a sudden decrease in the gas density, but also, in agreement with our results, the density of the gas at that radius was higher than the star formation threshold imposed in their simulations. In their work, the decrease in the stellar density was due to an angular momentum limitation. By construction, in their simulations, the angular momentum is directly proportional to the radius, which means that the high-angular-momentum material will take longer to cool. Therefore, the angular momentum determines the maximum extent of the gaseous disc and of the star-forming disc. In fully cosmological simulations, however, the accretion of matter is not as regular as the classical model of spherical shells collapsing from increasingly large radii. Particularly, at high redshift, before the galaxy is large enough to shock the accreting gas, accretion of gas occurs along filaments, as well as in mergers and clumps. The growth of our simulated disc is thus significantly more complicated than the disc in Roškar et al.'s idealized models. Although our disc does grow 'inside-out', it does so in a less regular manner. In our simulations, in fact, the gaseous disc extends beyond the stellar disc, and while in *some* time-steps the position of the break coincides with a change of slope in the surface gas density profile, this is not true at *all* time-steps.

Ferguson et al. (1998) proposed that the breaks in the star formation density could be due to an intrinsic correlation between azimuthally averaged SFR and gas volume density, combined with a vertical flaring of the disc or a warp, in such a way that the transformation between gas surface density and volume density varies with Galactocentric radius (Madore, van den Bergh & Rogstad 1974). We plot, in Fig. 13, the ratio between the surface density and the volume density of the gas in our simulated galaxy. It can be seen that, indeed, there is a change in the slope of this ratio at (approximately) the break radius.

Drops in the surface density of the gas at the onset of a warp have been observed in several galaxies (García-Ruiz, Sancisi & Kuijken 2002; Józsa 2007). In fact, a possible connection between truncated profiles and gaseous warps has been suggested several times in the literature (van der Kruit 2007). Fig. 14 shows the edge-on projection of the gas density distribution of our disc at three different redshifts, matching those of Fig. 4. The break radius coincides with the onset of a warp in the gaseous distribution in each of these three time-steps. Therefore, the decrease in the gaseous volume density due to this flaring seems to be a fundamental mechanism responsible for the break seen in the average SFR and, hence, the break in the light profile.

The coincidence of the initiation of the warp with the break radius at different time-steps is an encouraging piece of evidence in support of this suggestion. Having said that, this is but one simulation; a definitive statement awaits the analysis of a systemic suite of 20–30 comparable simulations, sampling a range of environments, assembly histories and dynamical masses – such an ambitious programme is currently underway within our group.

6 RADIAL MIGRATION

Fig. 15 compares the final (at z=0) Galactocentric radii for stars in our simulated disc ($R_{\rm final}$) with the radius at which they were formed ($R_{\rm initial}$). The right-hand panel shows the same distribution, but only for those stars outside the break radius. Using disc stars with $R_{\rm br} < r < 15$ kpc, we find that ∼57 per cent of the stars formed inside the break radius, ∼21 per cent formed *in situ* and ∼22 per cent formed

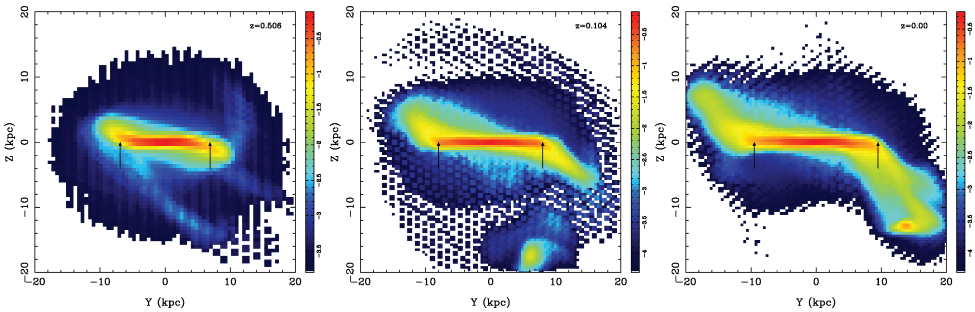

Figure 14. Edge-on projections of the logarithmic hydrogen density in H cm^{-3}, at three different redshifts (noted in the inset to each panel). Vertical arrows indicate the position of the break in the associated V-band stellar surface brightness profiles.

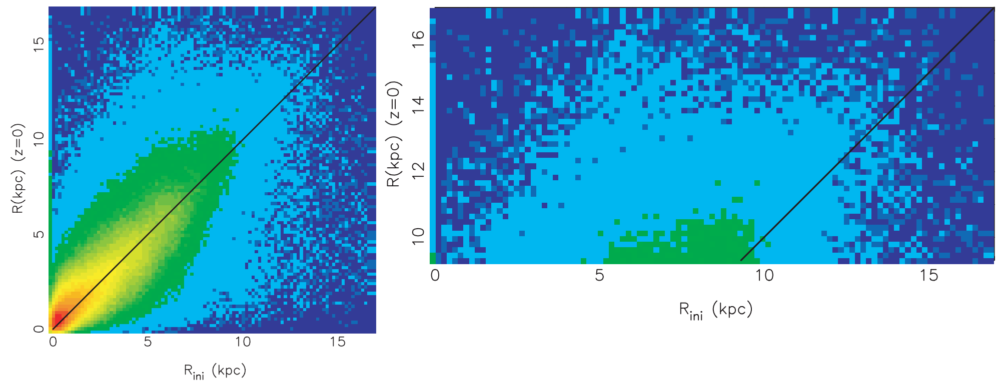

Figure 15. Final stellar Galactocentric radius versus formation radius. The different panels correspond to different scalings on the abscissa.

at $r > 15$ kpc or $|z| > 3$ kpc, including those formed elsewhere in external satellites – i.e. more than half of the stars currently in the outskirts of the disc formed at lower radii.

The mean radial distance traversed by the disc star particles (all those with $3 < r < 15$ kpc and $|z| < 3$ kpc, discounting those formed in satellites for this calculation) is $\langle|R_{\rm final} - R_{\rm initial}|\rangle =$ 1.7 kpc, while for those with $R_{\rm br} < r < 15$ kpc, this mean radial traversal distance is 3.4 kpc. It is clear that in our simulation there is considerable radial migration of stars towards the external parts. The importance of such radial migration and mixing within the thin disc has been the subject of several important studies (e.g. Spitzer & Schwarzschild 1953; Barbanis & Woltjer 1967; Fuchs 2001; Sellwood & Binney 2002; Haywood 2008; Roškar et al. 2008b).

It has been known for a number of years that scattering by spiral structure and molecular clouds can gradually heat stellar discs, moving stars towards more inclined and eccentric orbits and changing the overall angular momentum distribution of the disc. Minor mergers and accretion of satellites can also produce heating (e.g. Velazquez & White 1999, amongst many others). Stars that are on eccentric orbits are at different radii at different phases of their orbits and, therefore, tend to naturally produce some radial mixing. However, the radial excursions due to this mechanism are not sufficient to explain the flat age–metallicity relation in the solar neighbourhood (Sellwood & Binney 2002). Typical radial variations for a population of stars with a radial velocity dispersion σ_r are $\Delta R \sim \sqrt{2}\sigma_r/k$, where k is the epicyclic frequency; for the old stars in the Milky Way, the maximum value for the excursions near the Sun is ∼1–1.5 kpc.

Another proposed mechanism for radial migration was called 'churning' by Sellwood & Binney (2002), and is due to scattering of stars across corotation resonance by spiral waves (Sellwood & Binney 2002; Sellwood & Kosowsky 2002; Sellwood & Preto 2002; Roškar et al. 2008b), resulting in a change in the orbit centres, but not the eccentricity. Such churning causes little increase in random motions (or heating) because it preserves the overall distribution of angular momentum (see Sellwood & Binney 2002 for details). In the work of Roškar et al. (2008b), it was this churning mechanism that was predominantly responsible for the radial migration.

Our cosmological disc (as all hydrodynamical cosmological discs to date have been) is significantly hotter than that of the Milky Way (Gibson et al. 2008); as such, radial excursion of stars in eccentric orbits is no doubt contributing to (and perhaps dominating) the mixing. In fact, the epicyclic radius of the outer disc particles is 3.3 kpc, compatible with the mean calculated ΔR. We expect radial churning to have an important contribution too, although due to the larger scaleheight of our disc, this contribution is certainly less important than in Roškar et al. (2008b). Furthermore, our cosmological disc is continuously being bombarded by small satellites. Younger et al. (2007) showed that merger-driven gas inflows deepen the central potential and contract the inner profile while, at the same time, angular momentum is transferred to large radius and causes the outer disc to expand. This has the net effect of driving radial migration of the stars towards the external parts. It is very difficult to disentangle all the different causes of radial migration in our cosmological disc,[5] although it is certainly the case that each of these mechanisms is playing a role in both our simulated disc and real galaxies. The main heating mechanisms in the disc presented here and in other cosmological simulations will be the subject of a future paper (House et al., in preparation).

[5] Indeed, due to the large velocity dispersion of the stars compared with the Milky Way and to the larger scaleheight, cosmological simulations may not be the most appropriate for studying these particular mechanisms.

Roškar et al. (2008a) showed that radial migration due to this churning mechanism was able to explain the exponential decay of the surface brightness profile beyond $R_{\rm br}$, the constancy of the break radius for stars of different ages, and predict age profiles in agreement with observations (Bakos et al. 2008). The simulation of Roškar et al. (2008b) was performed under idealized conditions, with the disc growing *by construction* in an inside-out fashion, with very little star formation outside $R_{\rm br}$ (which itself increases monotonically with time). Hence, the stars beyond the break in their model *must* have migrated there. While these controlled, high-resolution simulations are *necessary* to study many of dynamical processes having place on the disc, it is also interesting (and important) to study the evolution of the surface brightness profile within a fully cosmological context, where hot and cold modes of gas accretion, and the effects of mergers and interactions are included. We find that the break radius does not always increase monotonically with time (see e.g. Fig. 11) and the shape of the final profile is influenced by a variety of external processes. Therefore, in the next section, we explore the effect of radial migration on the overall properties of our simulated disc.

7 IMPLICATIONS OF RADIAL MIGRATION FOR DISC PROPERTIES

7.1 Density profile

What is the effect of the radial migration in the density profile of our simulated disc? Fig. 16 shows the mass density profile at $z = 0$ compared with the hypothetical density profile that we would observe if the stars had not migrated from their birth place. The most dramatic changes in the density profile happen in the outer parts. The movement of the stars tends to weaken the intensity of the break that would have otherwise been seen in the stellar mass density profile.

This behaviour is quite different to what is seen in the simulations where the redistribution of angular momentum is caused by a bar (e.g. Foyle, Courteau & Thacker 2008). Foyle et al. found that the outer profile in their simulations barely changed with time, while the inner profile became flatter due to the redistribution of material. Nevertheless, Pohlen & Trujillo (2006) distinguish two types of Type II profiles – those associated with the OLR, and thus linked with the presence of a bar, and those not associated with bars, which are normally located at large radius (see Erwin et al. 2008 for a more detailed discussion). It may well be that two different mechanisms are responsible for these two variants of the Type II profiles. The profiles not associated with the OLR are less common in early-type galaxies than late-type galaxies (Pohlen & Trujillo 2006), which may indicate that the presence of an extended gaseous disc is necessary to produce them.

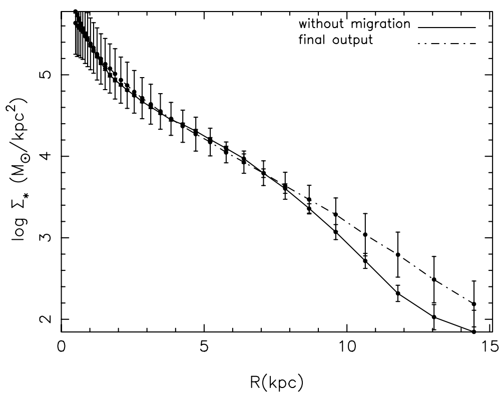

Figure 16. Stellar surface brightness density profile of the disc at $z = 0$ (dot–dashed curve) compared with the profile the disc would possess in the hypothetical situation that the redistribution of stellar material by secular processes was absent.

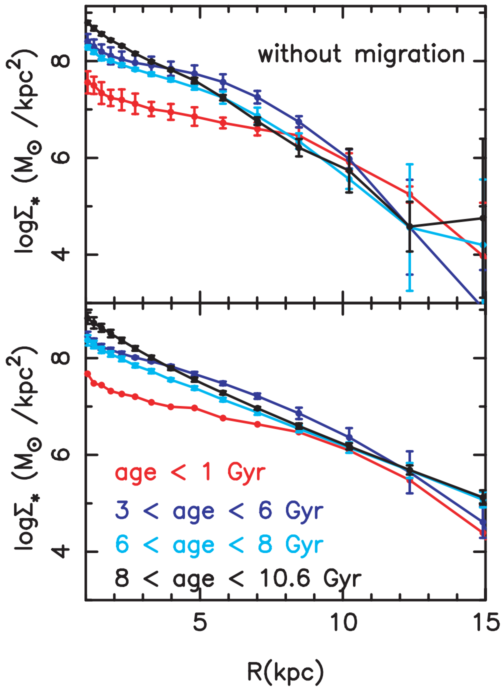

Figure 17. As in Fig. 16, but subdividing the stars by age, as indicated in the inset to each panel; upper panel: hypothetical situation of no radial migration; lower panel: as measured in our cosmological simulation.

We showed, in Section 4.2, that the old stars have a density profile with an upturn in the outer parts. Fig. 17 demonstrates that this is partially due to the significant effect that migration has on this outer profile. In this figure, the stellar density profile using different age bins is compared with the same profiles in the hypothetical situation where the stars have not migrated from the place of their birth. It is readily apparent that the surface density profile, in the absence of migration, appears truncated in all cases. This contrasts with the mass density profiles that we derived from the final output of our simulation, which appear much closer to a pure exponential (to at least ∼5 exponential scalelengths).

We conclude, therefore, that the exponential mass density profile in Fig. 4 would appear truncated/broken if there had not been radial migration. As old stars have had more time to migrate towards the external parts, the density profile for the oldest age bin appears antitruncated. This mechanism could also be responsible for the upbending profiles seen in galaxies where a truncation in the star formation density does not occur (Type III profiles, recalling the nomenclature of Section 1). This was also proposed by Younger et al. (2007) who found that in their simulations, the radial migration was produced by angular momentum transfer during minor mergers; such a scenario receives support from the empirical evidence associating asymmetries and distortions with antitruncated discs (Erwin et al. 2005; Pohlen & Trujillo 2006). As mentioned in Section 6, several mechanisms are certainly operating in our disc, in order to produce the radial migration of stars towards the external parts, including this effect of satellite accretion.

7.2 Stellar populations

Stars and interstellar gas in galaxies exhibit diverse chemical element abundance patterns that are shaped by their environment and formation histories. A wealth of surveys and satellite missions are devoted to obtain chemical patterns for individual stars as well as ages and kinematics in order to derive the star formation history and merger history of our galaxy (e.g. *Hipparcos*, RAVE, SEGUE, GAIA). The comparison with chemical and chemodynamical evolution models is expected to provide insights into the formation epoch of the different Galactic components and the relation between them.

Chemical evolution models of the Milky Way usually divide the 'Galaxy' into annuli with no radial transfer of material between them (e.g. Chiappini, Romano & Matteucci 2003; Fenner & Gibson 2003). However, recent works (e.g. Haywood 2008; Roškar et al. 2008b; Schönrich & Binney 2009) have pointed out the importance that migration mechanisms might have in the studies of chemical evolution, in particular upon the observational constrains used to calibrate the models. For example, one of the most difficult observational results to reproduce with current 'semi-numerical' chemical evolution models is the lack of an apparent correlation between the age and the metallicity of the stars in the solar neighbourhood, as well as the large scatter in metallicity at a given age. On the other hand, full chemodynamical models indicate that radial migration might be an explanation to this lack of correlation. Roškar et al. (2008a) have shown that radial migration can largely affect the age and metallicity gradients, as well as the dearth of metal-poor stars in the solar neighbourhood (the so-called 'G-dwarf problem'). It has even been suggested that radial migration might be responsible for the formation of the thick disc (e.g. Haywood 2008; Schönrich & Binney 2009).

These studies provide the motivation to re-examine the stellar population distribution within our simulated disc, where infall of material and the accretion of satellites are taken into account naturally within our cosmological framework.

7.2.1 *The age–metallicity relation*

Chemical evolution models predict an increase of the metal content in the ISM as stellar generations die and pollute their surroundings with the byproducts of nucleosynthesis. One might expect therefore that the youngest (oldest) stars would also be the most metal-rich (metal-poor). However, there is little evidence of such an age–metallicity relation in the solar neighbourhood (Feltzing, Holmberg & Hurley 2001; Nordström et al. 2004). Furthermore, the scatter in the relation is very large – i.e. at a given age, there is a large spread in the metallicity distribution. Classically, this was interpreted as a result of inefficient mixing of stellar ejecta. However, several authors (e.g. Wielen, Fuchs & Dettbarn 1996; Sellwood & Binney 2002) have suggested the possibility that radial migration may have enabled old stars, formed at small Galactocentric radii, to appear in the solar neighbourhood, flattening any correlation between age and metallicity. Roškar et al. (2008a) and Schönrich & Binney (2009) have shown that a flatter age–metallicity relation and a large spread in metallicities at a given age can be obtained with dynamical models where radial mixing is taken into account. Haywood (2006, 2008) observed that stars in the metal-poor and metal-rich ends of the thin disc have orbital parameters which are offset from the main population, which he interpreted as being the consequence of radial migration.

Fig. 18 shows the age–metallicity relation in the 'solar neighbourhood' ($7 < r < 9$ kpc and $|z| < 3$ kpc) of our simulated disc,

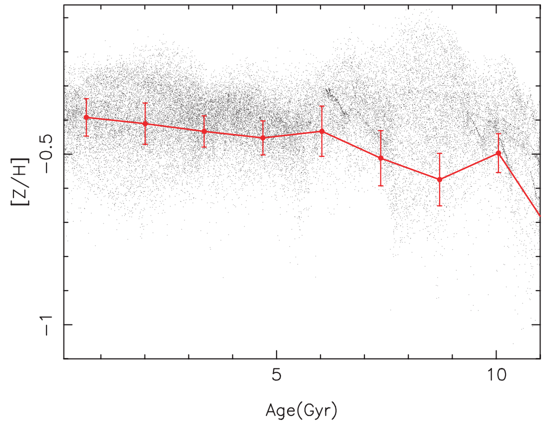

Figure 18. Age–metallicity relation for stellar particles with radius between 7 and 9 kpc and scaleheight $|z| < 3$ kpc, chosen to represent a region roughly corresponding to the 'solar neighbourhood'. The red points indicate the values derived for the stars born in this region.

compared with the age–metallicity relation that we would have measured in the absence of migration. As can be seen, our fully cosmological study is in agreement with the aforementioned idealized models. Radial migration produces a considerable flattening, and an increase of the scatter, in the age–metallicity relation. In the absence of radial migration, the stars in the solar neighbourhood of our disc would show a relation between these two parameters.

7.2.2 *Age gradient*

We showed, in Section 4.4, that the radial age profile has a minimum at the break radius, similar to that found by Roškar et al. (2008a). In their work, the radial extent of the star-forming disc was limited by the maximum angular momentum of material that was able to cool at each time-step. Therefore, by construction, the disc grows inside-out and the youngest stars are situated at the break radius. The 'upbend' in the age profile at $r > R_{\rm br}$ was produced, exclusively, by stars that had migrated from the internal parts of the disc. Because older stars have more time to travel larger distances, the trend of the age with radius reversed after the break radius.

To explore if this is also true in our simulation, we plot, in Fig. 19, the mass-weighted age profile that the stellar disc would have if the stars did not migrate from their birth place, compared with that derived from the final at $z = 0$. As can be seen, even in the absence of radial migration, a 'U-shape' profile in the age gradient is still visible. Stellar migration changes the shape of this profile, but the increasing mass-weighted age with increasing radius in the outer parts is *not* due to radial migration. Fig. 20 shows the evolution with time of the total SFR density for stars formed at different Galactocentric radii, including regions inside and beyond the break radius. For radii $3 < r < 5$ kpc, the SFR density decreases with time, while the opposite happens for $5 < r < 7$ kpc. The consequence of this is that the fraction of young-to-old stars increases with radius until $r = R_{\rm br}$, consistent with expectations, as the early accreted mass has low specific angular momentum. These trends are responsible for the decreasing mean age with radius and are in agreement with the inside-out scenario for the formation of disc galaxies (Ryder & Dopita 1994). However, the trend disappears beyond the break radius, where the SFR is low and essentially constant throughout the evolution of the galaxy. The difference in the SFR between the outer ($10 < r < 15$ kpc) and inner ($7 < r < 9$ kpc) parts is higher at later times, and that is the main reason for the upturn in the age

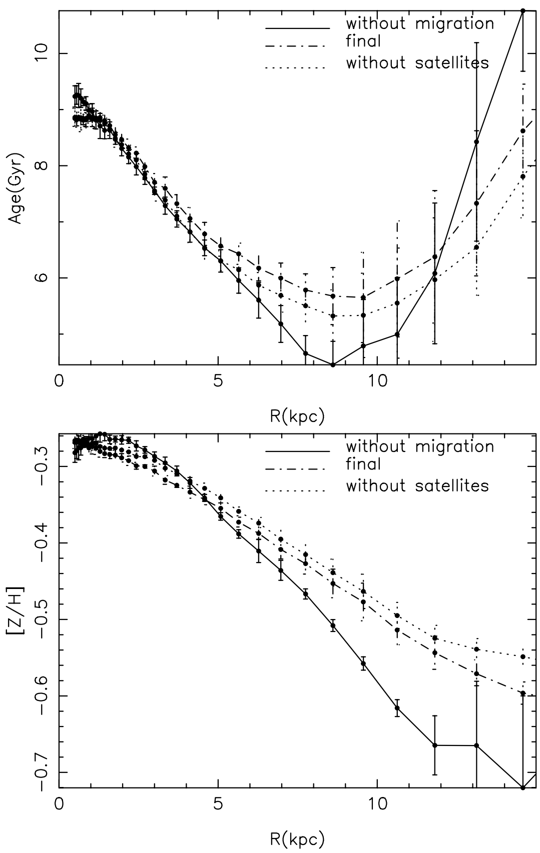

Figure 19. Mass-weighted azimuthally averaged stellar age and metallicity gradients. Solid lines: theoretical gradient for the hypothetical case where stars do not migrate from their birth place. Dash–dotted line: profile measured in the final time-step of our simulation. Dotted line: profile measured in the final time-step of the simulation after eliminating those stars which formed outside the disc (those with initial Galactocentric radii in excess of 25 kpc).

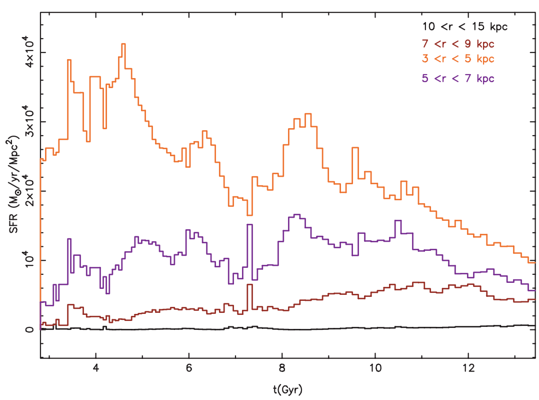

Figure 20. Comparison of the SFR density with time in four different regions of the galaxy disc – black: between 10 and 15 kpc; dark red: between 7 and 9 kpc; purple: between 5 and 7 kpc and orange between 3 and 5 kpc.

gradient Another way to appreciate this is by studying the radial profile of the birth parameter, defined as the current versus averaged star formation rate $b = (\mathrm{SFR}/\langle\mathrm{SFR}\rangle)$ (Kennicutt, Tamblyn & Congdon 1994). Instead of plotting the current SFR, we averaged the star formation over the last 1 Gyr. This is mainly due to the relative few number of particles with ages below this value outside the break radius. We plot, in Fig. 21, this parameter as a function of

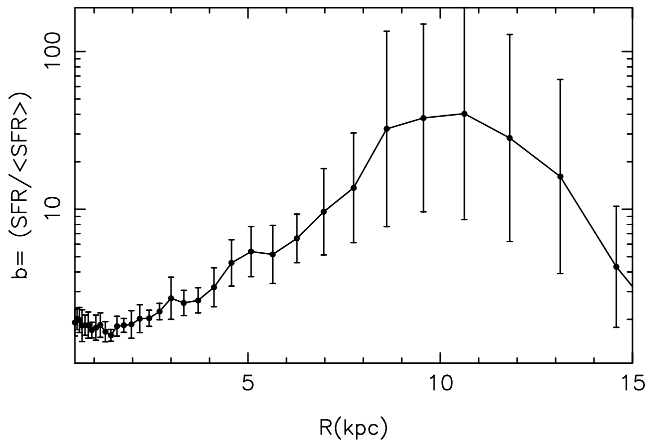

Figure 21. Star formation over the last 1 Gyr divided by the total mass of stars formed before this epoch (the so-called 'birth rate') as a function of Galactocentric radius.

Galactocentric radius. As can be seen, b increases almost linearly with radius, as expected for an inside-out formation scenario, until the break radius, where it reaches a plateau and then decreases. The increase in the error bars at the break radius reflects the asymmetries in the age distribution of the stars beyond this radius (recall Fig. 5).

We argue that the U-shape age profile is the direct consequence of the existence of a break in the star formation density. If the star formation outside the break had not decreased suddenly, the age gradient would decrease, or remain constant, until the edge of the optical disc. This is supported by the result of Bakos et al. (2008) who only found the telltale U-shaped colour profiles for galaxies possessing a Type II profile. The galaxies with an essentially pure exponential profile within their sample showed a plateau (and not an upbend) in the colours at large radii. This upbending age profile does not mean that the disc did not form inside-out. In fact, the 'overall' formation of the disc remains inside-out. However, in our disc, the decrease of star formation in the external parts – due to a decrease in the volume density of the gas – results in redder colours beyond the break radius.

In Fig. 19, we also compare the age profile of the galaxy with the one it would have if *all* the stars formed in the disc – i.e. if satellites were not accreted. It is apparent that for this case, the accretion of satellites has little effect on the stellar population gradients.

7.2.3 Metallicity gradient

The metallicity gradient in the disc and its evolution with time provide constraints to our understanding of the formation and evolution of galaxies. The presence of a metallicity gradient in the Milky Way is widely accepted, although its exact slope and shape remain contentious (Chiappini, Matteucci & Romano 2001; Andrievsky et al. 2002). A related issue is the evolution of this gradient with time; this has been approached from both the theoretical (Goetz & Koeppen 1992; Koeppen 1994; Molla, Ferrini & Diaz 1997; Henry & Worthey 1999; Chiappini, Matteucci & Romano 2001) and observational perspectives (Maciel 2001; Friel et al. 2002; Maciel, Costa & Uchida 2003; Stanghellini et al. 2006), but it is still not clear whether the metallicity gradient in our Galaxy flattens or steepens with time. Measurements using H II regions, B-stars and planetary nebulae find gradients ranging from ~ -0.04 to ~ -0.07 dex kpc^{-1} (Afflerbach, Churchwell & Werner 1997; Gummersbach et al. 1998;

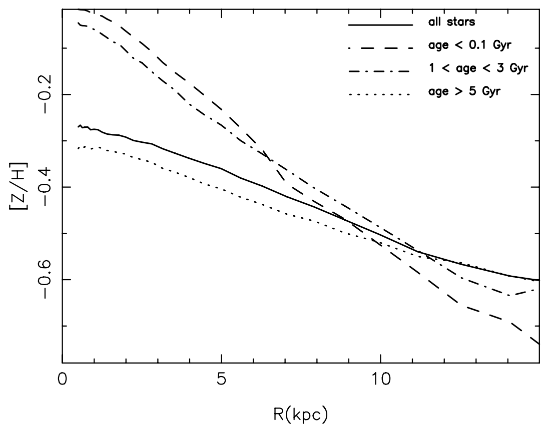

Figure 22. Azimuthally averaged metallicity profile at redshift $z = 0$ for stars in different age bins, as noted in the inset.

Maciel & Quireza 1999; Deharveng et al. 2000; Costa, Uchida & Maciel 2004; Daflon & Cunha 2004, although see Stanghellini et al. 2006). Even more recently, Carraro et al. (2007), using five old open clusters, suggest an even shallower gradient of -0.018 dex kpc^{-1}. There is also controversy in the literature about the shape of the gradient, including the presence or not of a discontinuity at around 10–12 kpc. Part of the uncertainty in this field can no doubt be traced to the necessary use of disparate tracers of the gradients, each which probe a different age (or range of ages).

In our simulations, we find that the metallicity gradient is flatter for old stars than it is for young stars, as shown in Fig. 22. It can also be seen that radial migration is partially responsible for this flattening (see Fig. 19), in agreement with Roškar et al. (2008a). We also predict that the optimal Galactocentric radius in which to seek differences between the gradients in the old versus young populations is $3 < r < 5$ kpc. As can be seen in Fig. 19 (lower panel), the mean metallicity gradient in our simulation shows a flattening at $r > 12$ kpc.

8 DISCUSSION AND CONCLUSIONS

We have studied the origin of the disc truncations and the stellar population properties of a disc galaxy formed within a cosmological framework. To do this, we have analysed a multiresolved cosmological simulation of a Milky Way mass halo, including dark matter and gas dynamics, atomic and metallicity-dependent cooling, UV heating, star formation and supernovae feedback, using the AMR code RAMSES. Our simulated disc shows a break in the surface brightness profile at ∼3 exponential scalelengths, similar to those observed in a large fraction of disc galaxies. The position of the break does not coincide with the radius at which the gas density reaches the canonical threshold for star formation. In our simulation, this break in the stellar light is due to a decrease in the star formation density per area unit (averaged over the past ∼1 Gyr). This decrease in the star formation density originates from a decrease in the volume density of gas at the break radius, which itself coincides with the radius at which the gas disc begins to warp ($R_{\rm warp}$). A relationship between truncations and warps has been pointed out by several studies (see van der Kruit 2008 for a review as well as van der Kruit 2001). van der Kruit (2007) found that the distribution of $R_{\rm warp}/R_{\rm br}$ in a sample of SDSS galaxies was statistically consistent with all warps starting at ∼1.1 $R_{\rm br}$. Our simulation is entirely consistent with these observations. At a first sight, therefore, it seems that the presence of a warp is a condition for the presence of a break in the stellar light distribution. However, we reiterate that this need to be confirmed with a larger sample of simulated and observed discs.

We analysed the redistribution of material and angular momentum in the disc, finding that it considerably affects the final shape of the mass density profile, especially in the outskirts. In fact, 57 per cent of the stars with $r > R_{\rm br}$ formed at lower radii. The reason why the surface density profile does not show a truncation similar to the one observed in the stellar light is traced to this migration of stars towards the outer disc. We suggest that truncated and antitruncated profiles can be produced by a different combination of two processes: (1) a change in the slope of star formation profile with radius due to a change of the slope in the gas density profile (which causes the truncation in the light) and (2) radial migration of stars formed in the internal parts towards radii in excess of $R_{\rm br}$. We speculate that upbending profiles can be produced in our simulation when the distribution of the gas changes smoothly with radius. In that case, process (1) is suppressed, the SFR per area unit in the disc changes smoothly with radius and the only deviations from a pure exponential profile are due to stars migrating from disc interior, producing an increase in both the surface light and mass density in the external parts. This would make the external parts somewhat redder, in agreement with observations (Bakos et al. 2008). Pure exponential profiles can be similar to antitruncated profiles, but with less migration.

We have also studied the stellar populations in the disc and the influence of the migration of stars and the accretion of satellites in the age and metallicity profiles. We found, in agreement with recent observations (Bakos et al. 2008), that the disc shows a U-shaped age profile, reaching the minimum age at the position of the break. It has been proposed in recent works that this profile is produced by the combination of two processes: (1) the inside-out growth of the disc (resulting in the age decreasing with radius until $R_{\rm br}$) and (2) the migration of old stars from the interior to the exterior parts of the disc beyond $R_{\rm br}$. In this picture, the increase of age with radius beyond the break results from older stars having more time to travel from the inner disc and, therefore, reach a greater Galactocentric radius. These models predict a flat metallicity gradient for the old stellar populations, as these stars are mixed very efficiently. In our simulation, the U-shaped profile is due to a different rate of star formation between the internal and the external regions (inside and outside the break radius). Migration of the stars also has an impact on this profile, but the U-shape age profile with the minimum at the break radius appears even when migration is suppressed in the disc. We find that the U-shaped age profile is due to the same mechanism as the one producing the break in the surface brightness distribution – i.e. a diminution of the SFR in the external region, due to the warping of the gaseous disc, and therefore we predict that this type of colour profile is only present when there is a break in the light distribution. This is in agreement with the recent work of Bakos et al. (2008), at low redshifts, and Azzollini et al. (2008) at redshifts out to $z \sim 1.1$.

The distribution of ages in the outer disc of our simulation is very broad with stars nearly as old as the age of the Universe itself. The presence of old stars (>10 Gyr) in the outer disc of some nearby galaxies, such as M31 (Ferguson & Johnson 2001), has been used as an argument against ΛCDM models, arguing that, if feedback is included in order to produce large discs, the formation of the disc is delayed and the resulting stellar populations should be of young and intermediate ages. We show here that in a ΛCDM framework we were able to produce disc with both a realistic scalelength and a considerable number of old stars in its external parts. The metallicity distribution of stars in the outskirts of the disc peaks at

[Fe/H] ~ -0.5 and also shows a significant spread, also consistent with observations.

Finally, we studied the age–metallicity relationship in a representative 'solar neighbourhood' of our simulation. There have been claims suggesting that radial mixing of stars might be responsible for the absence of an obvious correlation between these two parameters in the solar neighbourhood, and for the large scatter in metallicity at a given age. We agree with these claims, showing that a flat relationship between age and metallicity, and significant scatter in metallicity at a given age, is a natural outcome within our cosmological simulation.

In a forthcoming paper, we will study the origin of the warp in the gaseous distribution, its lifetime, asymmetry and intensity. This will be supplemented with a suite of 20–30 additional disc simulations, spanning a range of mass, environment and assembly history. This will allow us to provide significantly more robust predictions for the relationship between break radii and other empirical characteristics of galaxies.

ACKNOWLEDGMENTS

We wish to thank Romain Teyssier, Ignacio Trujillo, Armando Gil de Paz and Isabel Pérez for their constant and extremely enlightening advice. We thank Ruyman Azzollini for providing his data in tabular form and the referee of this paper, Dr Peter Erwin, for useful comments that have improved the presentation of the manuscript. We also thank Victor Debattista and Rok Roškar for useful comments that significantly improved the manuscript. PSB acknowledges the support of a Marie Curie Intra-European Fellowship within the 6th European Community Framework Programme. BKG acknowledges the support of UK's Science & Technology Facilities Council (STFC Grant ST/F002432/1) and the Commonwealth Cosmology Initiative. All modelling and analyses were carried out on the University of Central Lancashire's High Performance Computing Facility and UK's National Cosmology Supercomputer (COSMOS).

REFERENCES

Abadi M. G., Navarro J. F., Steinmetz M., Eke V. R., 2003a, ApJ, 591, 499
Abadi M. G., Navarro J. F., Steinmetz M., Eke V. R., 2003b, ApJ, 597, 21
Afflerbach A., Churchwell E., Werner M. W., 1997, ApJ, 478, 190
Andrievsky S. M., Kovtyukh V. V., Luck R. E., Lépine J. R. D., Maciel W. J., Beletsky Y. V., 2002, A&A, 392, 491
Azzollini R., Trujillo I., Beckman J. E., 2008a, ApJ, 679, L69
Azzollini R., Trujillo I., Beckman J. E., 2008b, ApJ, 684, 1026
Bailin J. et al., 2005, ApJ, 627, 17
Bakos J., Trujillo I., Pohlen M., 2008, ApJ, 683, L103
Barbanis B., Woltjer L., 1967, ApJ, 150, 461
Barton I. J., Thompson L. A., 1997, AJ, 114, 655
Beckman J. E., Irwin P., Pohlen M., 2006, in Ulla A., Manteiga M., eds, Proc. 2nd Astrophys. Symp., Lecture Notes and Essays in Astrophysics, Vol. 2. Spanish Ministry of Education and Science/Royal Spanish Physical Society, Madrid, pp. 199–214
Bell E. F., McIntosh D. H., Katz N., Weinberg M. D., 2003, ApJS, 149, 289
Bertelli G., Bressan A., Chiosi C., Fagotto F., Nasi E., 1994, A&AS, 106, 275
Bland-Hawthorn J., Vlajić M., Freeman K. C., Draine B. T., 2005, ApJ, 629, 239
Bruzual G., Charlot S., 2003, MNRAS, 344, 1000
Carraro G., Geisler D., Villanova S., Frinchaboy P. M., Majewski S. R., 2007, A&A, 476, 217
Chiappini C., Matteucci F., Romano D., 2001, ApJ, 554, 1044
Chiappini C., Romano D., Matteucci F., 2003, MNRAS, 339, 63
Costa R. D. D., Uchida M. M. M., Maciel W. J., 2004, A&A, 423, 199
Daflon S., Cunha K., 2004, ApJ, 617, 1115
Dalcanton J. J., Spergel D. N., Summers F. J., 1997, ApJ, 482, 659
Davidge T. J., 2003, AJ, 125, 3046
de Grijs R., Kregel M., Wesson K. H., 2001, MNRAS, 324, 1074
de Jong R. S. et al., 2007, ApJ, 667, L49
Debattista V. P., Mayer L., Carollo C. M., Moore B., Wadsley J., Quinn T., 2006, ApJ, 645, 209
Deharveng L., Peña M., Caplan J., Costero R., 2000, MNRAS, 311, 329
Dubois Y., Teyssier R., 2008, A&A, 477, 79
Elmegreen B. G., Hunter D. A., 2006, ApJ, 636, 712
Erwin P., Beckman J. E., Pohlen M., 2005, ApJ, 626, L81
Erwin P., Pohlen M., Beckman J. E., 2008, AJ, 135, 20
Fall S. M., Efstathiou G., 1980, MNRAS, 193, 189
Feltzing S., Holmberg J., Hurley J. R., 2001, A&A, 377, 911
Fenner Y., Gibson B. K., 2003, Publ. Astron. Soc. Aust., 20, 189
Ferguson A. M. N., 1998, PhD thesis, Johns Hopkins University
Ferguson A. M. N., Clarke C. J., 2001, MNRAS, 325, 781
Ferguson A. M. N., Johnson R. A., 2001, ApJ, 559, L13
Ferguson A. M. N., Wyse R. F. G., Gallagher J. S., Hunter D. A., 1998, ApJ, 506, L19
Ferland G. J., Korista K. T., Verner D. A., Ferguson J. W., Kingdon J. B., Verner E. M., 1998, PASP, 110, 761
Foyle K., Courteau S., Thacker R. J., 2008, MNRAS, 386, 1821
Freeman K. C., 1970, ApJ, 160, 811
Friel E. D., Janes K. A., Tavarez M., Scott J., Katsanis R., Lotz J., Hong L., Miller N., 2002, AJ, 124, 2693
Fuchs B., 2001, MNRAS, 325, 1637
Galleti S., Bellazzini M., Ferraro F. R., 2004, A&A, 423, 925
García-Ruiz I., Sancisi R., Kuijken K., 2002, A&A, 394, 769
Gibson B. K., Courty S., Sánchez-Blázquez P., Teyssier R., House E. L., Brook C. B., Kawata D., 2009, in Anderse J., Bland-Hawthorn J., Nordstrom B., eds, IAU Symp. 254, The Galaxy Disk in Cosmological Context. Cambridge Univ. Press, Cambridge, p. 445
Gil de Paz A., Madore B. F., Boissier S., Thilker D., Bianchi L., Sánchez Contreras e. A., 2007, ApJ, 661, 115
Goetz M., Koeppen J., 1992, A&A, 262, 455
Governato F., Willman B., Mayer L., Brooks A., Stinson G., Valenzuela O., Wadsley J., Quinn T., 2007, MNRAS, 374, 1479
Gummersbach C. A., Kaufer A., Schaefer D. R., Szeifert T., Wolf B., 1998, A&A, 338, 881
Haardt F., Madau P., 1996, ApJ, 461, 20
Haywood M., 2006, MNRAS, 371, 1760
Haywood M., 2008, MNRAS, 388, 1175
Henry R. B. C., Worthey G., 1999, PASP, 111, 919
Hunter D. A., Elmegreen B. G., 2006, ApJS, 162, 49
Jansen R. A., Fabricant D., Franx M., Caldwell N., 2000, ApJS, 126, 331
Józsa G. I. G., 2007, A&A, 468, 903
Juric M. et al., 2008, ApJ, 673, 864
Kennicutt R. C., Jr, 1989, ApJ, 344, 685
Kennicutt R. C., Jr., Tamblyn P., Congdon C. E., 1994, ApJ, 435, 22
Koeppen J., 1994, A&A, 281, 26
Kregel M., van der Kruit P. C., de Grijs R., 2002, MNRAS, 334, 646
Maciel W. J., 2001, New Astron. Rev., 45, 571
Maciel W. J., Quireza C., 1999, A&A, 345, 629
Maciel W. J., Costa R. D. D., Uchida M. M. M., 2003, A&A, 397, 667
Madore B. F., van den Bergh S., Rogstad D. H., 1974, ApJ, 191, 317
Maraston C., Thomas D., 2000, ApJ, 541, 126
MacArthur L. A., Courteau S., Holtzman J. A., 2003, ApJ, 582, 689
Mo H. J., Mao S., White S. D. M., 1998, MNRAS, 295, 319
Molla M., Ferrini F., Diaz A. I., 1997, ApJ, 475, 519
Navarro J. F., White S. D. M., 1994, MNRAS, 267, 401
Nordström B. et al., 2004, A&A, 418, 989
Okamoto T., Eke V. R., Frenk C. S., Jenkins A., 2005, MNRAS, 363, 1299
Patterson F. S., 1940, Harv. Coll. Obs. Bull., 914, 9
Peñarrubia J., McConnachie A., Babul A., 2006, ApJ, 650, L33
Pérez I., 2004, A&A, 427, L17
Pohlen M., 2002, PhD thesis, Ruhr-Universität Bochum

Pohlen M., Trujillo I., 2006, A&A, 454, 759
Pohlen M., Beckman J. E., Hüttemeister S., Knapen J. H., Erwin P., Dettmar R.-J., 2004, in Block D. L., Puerari I., Freeman K. C., Groess R., Block E. K., eds, Penetrating Bars Through Masks of Cosmic Dust, Vol. 319. Astrophysics and Space Science Library. Kluwer, Dordrecht, p. 713
Pohlen M., Zaroubi S., Peletier R. F., 2007, in Combes F., Palous J., eds, IAU Symp. 235, Galaxy Evolution Across The Hubble Time. Cambridge Univ. Press, Cambridge, p. 129
Rose J. A., 1985, AJ, 90, 1927
Roškar R., Debattista V. P., Quinn T. R., Stinson G. S., Wadsley J., 2008a, ApJ, 684, L79
Roškar R., Debattista V. P., Stinson G. S., Quinn T. R., Kaufmann T., Wadsley J., 2008b, ApJ, 675, L65
Ryder S. D., Dopita M. A., 1994, ApJ, 430, 142
Salpeter E. E., 1955, ApJ, 121, 161
Scannapieco C., Tissera P. B., White S. D. M., Springel V., 2008, MNRAS, 389, 1137
Scannapieco C., White S. D. M., Springel V., Tissera P. B., 2009, MNRAS, 396, 696
Schönrich R., Binney J., 2009, MNRAS, 396, 203
Sellwood J. A., Binney J. J., 2002, MNRAS, 336, 785
Sellwood J. A., Kosowsky A., 2002, in Da Costa G. S., Jerjen H., eds, ASP Conf. Ser. Vol. 273, The Dynamics, Structure & History of Galaxies: A Workshop in Honour of Professor Ken Freeman, Distinguishing Dark Matter from Modified Gravity. Astron. Soc. Pac., San Francisco, p. 243
Sellwood J. A., Preto M., 2002, in Athanassoula E., Bosma A., Mujica R., eds, ASP Conf. Ser. Vol. 275, Disks of Galaxies: Kinematics, Dynamics and Peturbations, Scattering of Stars by Transient Spiral Waves. Astron. Soc. Pac., San Francisco, p. 281
Simien F., de Vaucouleurs G., 1986, ApJ, 302, 564
Spitzer L. J., Schwarzschild M., 1953, ApJ, 118, 106
Springel V., Hernquist L., 2003, MNRAS, 339, 289
Stanghellini L., Guerrero M. A., Cunha K., Manchado A., Villaver E., 2006, ApJ, 651, 898
Teyssier R., 2002, A&A, 385, 337
Thilker D. A., Bianchi L., Boissier S. e. A., 2005, ApJ, 619, L79
Thilker D. A., Bianchi L., Meurer G. e. A., 2007, ApJS, 173, 538
Trager S. C., Worthey G., Faber S. M., Dressler A., 2005, MNRAS, 362, 2
Trujillo I., Pohlen M., 2005, ApJ, 630, L17
van den Bosch F. C., 2001, MNRAS, 327, 1334
van der Kruit P. C., 1979, A&AS, 38, 15
van der Kruit P. C., 1987, A&A, 173, 59
van der Kruit P. C., 2001, in Funes J. G., Corsini E. M., eds, ASP Conf. Ser. Vol. 230, Galaxy Disks and Disk Galaxies, Truncations in Stellar Disks. Astron. Soc. Pac., San Francisco, p. 119
van der Kruit P. C., 2007, A&A, 466, 883
van der Kruit P. C., 2008, in Funes J. G., Corsini E. M., eds, ASP Conf. Ser. Vol. 396, The Stars and Gas in Outer Parts of Galaxy Disks: Extended or Truncated, Flat or Warped? Astron. Soc. Pac., San Francisco, p. 173
Velazquez H., White S. D. M., 1999, MNRAS, 304, 254
Weiner B. J., Williams T. B., van Gorkom J. H., Sellwood J. A., 2001, ApJ, 546, 916
Wielen R., Fuchs B., Dettbarn C., 1996, A&A, 314, 438
Worthey G., 1994, ApJS, 95, 107
Younger J. D., Cox T. J., Seth A. C., Hernquist L., 2007, ApJ, 670, 269

APPENDIX A: DEPENDENCE OF THE BREAK RADIUS UPON INCLINATION

Recently, van der Kruit (2008) studied the correlations between break radius and other galaxy properties, finding fundamental differences between the trends described by face-on and edge-on galaxies. In particular, he did not find a correlation between the position of the break and the rotational velocity in the face-on sample, while the correlation was evident in the edge-on galaxies. In principle, breaks are more easily detected in edge-on galaxies, due to their favoured integrated line-of-sight vantage point. Face-on breaks are more difficult to detect, and if the truncation radius changes with azimuth, the azimuthally averaged profiles would 'smear out' the intensity of the break. Furthermore, intrinsic deviations from circular symmetry, such as spiral arms (especially for younger populations), should complicate matters for less inclined systems. On the other hand, edge-on studies are more susceptible to line-of-sight effects caused by integrating through the disc. The differences between the parameters measured in face-on and edge-on samples can be obtained statistically, but obviously, they are difficult to quantify. In this Appendix, we compare the break radius and the intensity of the break in different bands by viewing our simulation various face-on and edge-on configurations, in order to quantify possible differences due to geometry. Differences due to the varying dust contribution with inclination cannot be treated here, but we refer the reader to Pohlen, Zaroubi & Peletier (2007) for a thorough analysis of this issue.

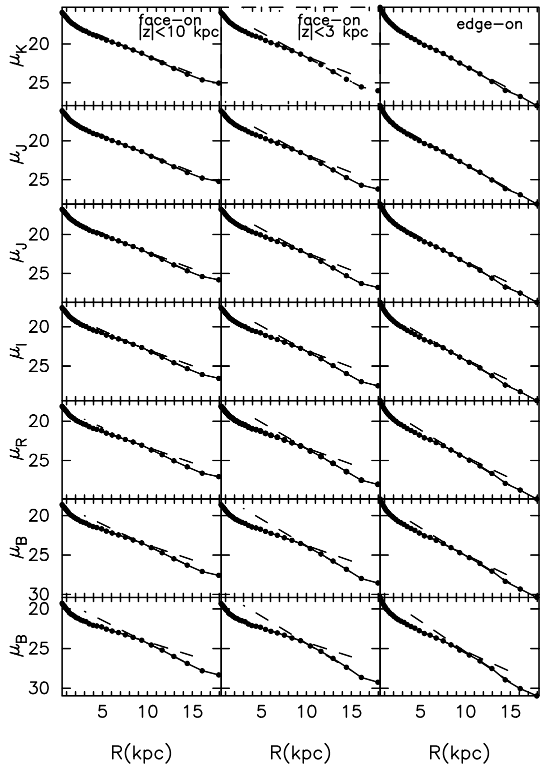

Figure A1. Surface brightness profiles in different bands calculated in face-on (azimuthally averaging) and edge-on configurations. For the face-on projection, we have integrated between different distances from the disc mid-plane, as indicated in the inset.

All the profiles previously showed in this work have been obtained by azimuthally averaging the luminosities of the stars within 3 kpc of the disc mid-plane. Observers, of course, integrate their luminosities along the entire line of sight. In order to mimic this, we compare the profiles integrating the light of all stars within a distance of 10 kpc from the disc mid-plane. Fig. A1 shows the surface brightness profiles in different bands obtained for face-on and edge-on orientations. Table A1 shows the measured values for the position of the break and the angle between the two exponential fits in each configuration.

We do not find any fundamental difference between the position of the break or its intensity for the face-on and edge-on values; they agree, within the uncertainties. The table also shows the measured inner and outer scalelengths. The uncertainties in the measurement

Table A1. Break radius and angle between the two exponential fits in different bands.

	Band	Face-on $\|z\| < 10\,\mathrm{kpc}$	Face-on $\|z\| < 3\,\mathrm{kpc}$	Edge-on
R_{br}	B	9.3 ± 0.3	9.6 ± 0.7	9.8 ± 1.0
h_{inn}	B	2.83	2.75	1.95
h_{out}	B	1.74	1.46	1.30
Angle	B	10.2	14.4	10.4
R_{br}	V	9.2 ± 0.4	9.5 ± 0.6	9.3 ± 1.3
h_{inn}	V	2.61	2.53	1.81
h_{out}	V	1.83	1.47	1.41
Angle	V	7.6	12.5	6.3
R_{br}	R	8.9 ± 0.7	9.8 ± 0.4	9.2 ± 1.7
Angle	R	5.9	11.1	6.5
h_{inn}	R	2.51	2.43	1.83
h_{out}	R	1.90	1.52	1.42
R_{br}	I	8.7 ± 1.1	9.6 ± 0.4	8.3 ± 1.0
Angle	I	4.6	9.3	4.2
h_{inn}	I	2.42	2.34	1.80
h_{out}	I	1.96	1.57	1.52
R_{br}	J	8.2 ± 1.7	9.5 ± 0.3	7.8 ± 1.4
Angle	J	3.4	8.2	3.4
h_{inn}	J	2.31	2.24	1.76
h_{out}	J	1.99	1.58	1.54
R_{br}	H	8.1 ± 2.9	9.5 ± 0.3	12.1 ± 6.0
h_{inn}	H	2.20	2.20	1.60
h_{out}	H	2.00	1.59	1.52
Angle	H	2.1	7.7	1.3
R_{br}	K	9.2 ± 2.1	9.4 ± 0.3	–
h_{inn}	K	2.22	2.19	1.65
h_{out}	K	1.95	1.58	1.55
Angle	K	2.8	7.7	0

of the scalelength are <0.1 per cent and are, therefore, not listed. We can see that contrary to what happens with the position of the break, we did find differences in the scalelengths of the disc when measured at different inclinations. In particular, the scalelengths are systematically lower in the edge-on projections, counter to that claimed by van der Kruit (2008). Due to the smaller scalelength obtained in edge-on systems, the R_{br}/h measured for this projection is larger than for the face-on projection. These differences have been found previously in empirical studies, but it is not clear if they are due to projection effects or due to different techniques to mark the break (see Pohlen & Trujillo 2006).

Finally, we do not find a sharper edge in edge-on galaxies than for face-on systems, for which we conclude that this effect, reported in observations, must be the consequence of dust extinction.

This paper has been typeset from a TEX/LATEX file prepared by the author.